Surface Science 234 (1990) 315–323
North-Holland

EQUILIBRIUM SHAPES OF CRYSTALS NEAR THE TRIPLE POINT

H. LÖWEN

Sektion Physik der Universität München, Theresienstrasse 37, D-8000 München 2, Fed. Rep. of Germany

Received 20 December 1989; accepted for publication 3 April 1990

The Wulff construction for the equilibrium shape of a crystal, being in coexistence with its vapor, is applied to a situation very near the triple point where the liquid phase becomes thermodynamically stable, too. This is particularly interesting if some planes of the crystal melt and other ones do not. In this case, it is found that the equilibrium shape exhibits liquid lenses on the crystal which match with a finite angle to the crystalline part. The results are compared with recent equilibrium shape measurements of lead crystallites.

1. Introduction

The problem to determine the equilibrium shape of a crystal, if its surface tension is given as a function of orientation, is very old and was formulated as a variational problem in the last century. In 1901, Wulff [1] answered this question giving an explicit geometric construction which is the Legendre transform of the surface tension with respect to the orientation angle. This was proved rigorously later on by Dinghas [2], for a review see Herring [3].

In the usual Wulff construction one considers a crystal in coexistence with its vapor, far away from the triple point where the liquid becomes a third stable phase. Therefore, a quite natural question concerns the application of the Wulff construction to a three-phase situation. One then starts from *three* given surface tensions (solid–gas, solid–liquid, liquid–gas), one of them (liquid–gas) being orientation-independent, and looks for the equilibrium shape which minimizes the total free energy.

This is also motivated by recent equilibrium shape measurements on lead crystallites near the melting temperature by Métois and coworkers [4–6] and by Pavlovska, Faulian and Bauer [7]. For lead, the interesting situation occurs that some planes (e.g. (110)) do melt and others (e.g. (111)) do not [8].

The experimental situation, however, is still somewhat inconclusive. There is clear evidence of surface melting of the looser packed planes, whereas it is still controversial how surface melting does influence the equilibrium shape of the crystal. In ref. [5], it is found that the equilibrium shape consists of facets and rounded parts. The matching of these parts becomes angular some 20 K below the triple temperature. The matching angle and the facet size increase with increasing temperature T. Pavlovska et al. [7], however, observed a ring around the (111) facet, which was not seen in ref. [5]. The width of the ring decreases with increasing T. As in ref. [5], the facet size increases with T. Another interesting experimental finding [6] is that facetted nonequilibrium crystals can be overheated, which is very unusual.

Recently, Nozières [9] made a qualitative study of the influence of surface melting on the equilibrium shape for two-dimensional crystals. In this work, the occurrence of liquid lenses and finite angular matching are explained qualitatively and several mechanisms which may produce the temperature-dependence of the matching angle and the facet size are proposed. Furthermore, superheating of a facetted crystal is explained and an estimation for the superheating temperature is given.

It is the aim of the present paper to understand generally the connection between the equilibrium

shape of a crystal near the triple point and the associated three surface tensions (solid–gas, solid–liquid, liquid–gas). A simple model is proposed where a generalization of Wulff's construction is possible in two dimensions and an attempt is made to compare quantitatively with the equilibrium shape measurements on lead crystallites.

The organization is as follows: First, we consider two-dimensional crystals. In section 2, a generalization of Wulff's construction is described and an illustration of the solution is given. For a simple model of a two-dimensional square lattice crystal, numerical results for the equilibrium shape are presented in section 3. As already obtained qualitatively by Nozières [9], it exhibits liquid lenses on the crystal which match with a finite angle to the crystalline part. In three dimensions, the situation is more complicated. This is briefly discussed in section 4. Then the theory is applied to lead. We adopt experimental data for the surface tension extrapolated to the triple point and calculate the equilibrium shape. This is compared with the experiments which were mentioned above.

2. Application of Wulff's construction to the triple point

In this section and in the following one, we consider two-dimensional crystals or – equivalently – cylindrical three-dimensional ones. Generalizations to three dimensions are addressed in sections 4 and 5. The orientation of a crystal plane can then be characterized by a single angle θ or by a two-dimensional unit vector $\hat{\boldsymbol{n}} = (\cos\theta, \sin\theta)$. Let $\gamma_{SV}(\hat{\boldsymbol{n}})$, $\gamma_{SL}(\hat{\boldsymbol{n}})$, γ_{LV} denote the surface tension between the solid/vapor, solid/liquid and liquid/vapor phases at the triple point. In contrast to γ_{SV} and γ_{SL}, γ_{LV} does not depend on orientation. If, for a given orientation $\hat{\boldsymbol{n}}$, the surface of the solid which is in equilibrium with its vapor is wetted by the liquid, $\gamma_{SV}(\hat{\boldsymbol{n}})$ is not well-defined. We then set $\gamma_{SV}(\hat{\boldsymbol{n}}) = \gamma_{SL}(\hat{\boldsymbol{n}}) + \gamma_{LV}$.

Consider now a situation sketched in fig. 1. In general, a two-dimensional crystal with an n-fold symmetry has a solid/vapor $z_1(x)$, solid/liquid $z_2(x)$ and liquid/vapor $z_3(x)$ interface which meet at a trijunction point with Cartesian coordinates

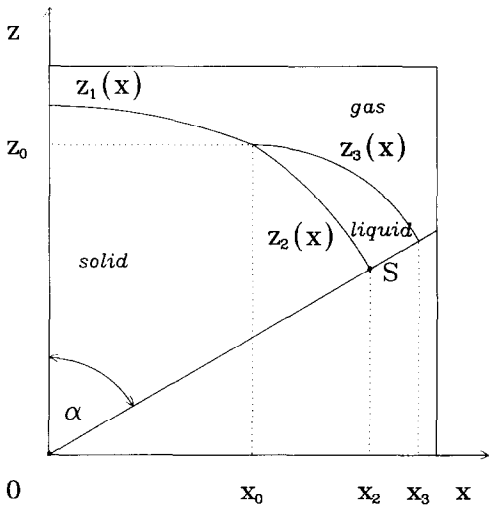

Fig. 1. Geometry of the situation and nomenclature. One sector of the crystal which has an n-fold symmetry is shown. Three kinds of interfaces occur: solid/vapor $z_1(x)$, solid/liquid $z_2(x)$, liquid/vapor $z_3(x)$. They meet at a trijunction (x_0, z_0).

(x_0, z_0). In fig. 1, only one sector of the crystal is shown with angle $\alpha = 2\pi/n$.

The problem then is to minimize the total surface free energy Σ,

$$\Sigma/n = \int_0^{x_0} \mathrm{d}x\, f_{SV}(z_1'(x)) + \int_{x_0}^{x_2} \mathrm{d}x\, f_{SL}(z_2'(x)) + \int_{x_0}^{x_3} \mathrm{d}x\, f_{LV}(z_3'(x)), \tag{1}$$

with the constraint of fixed total mass M of the solid/liquid system

$$M = \rho_S A_S + \rho_L A_L, \tag{2}$$

where

$$A_S/n = \int_0^{x_0} \mathrm{d}x\, z_1(x) + \int_{x_0}^{x_2} \mathrm{d}x\, z_2(x) - (x_2^2 \tan\alpha)/2, \tag{3}$$

$$A_L/n = \int_{x_0}^{x_3} \mathrm{d}x\, z_3(x) - \int_{x_0}^{x_2} \mathrm{d}x\, z_2(x) - \left[(x_3^2 - x_2^2)\tan\alpha\right]/2. \tag{4}$$

In eq. (1), the functions f_i are given by

$$f_i(p) = \gamma_i\left((p, 1)/\sqrt{1+p^2}\right)\sqrt{1+p^2}\,,$$
$$i = \mathrm{SV}, \mathrm{SL}, \mathrm{LV}, \tag{5}$$

and ρ_S and ρ_L are the densities of the solid and liquid, usually $\rho_S > \rho_L$. Furthermore, $z_i'(x) \equiv dz_i/dx$.

So far, a situation directly at the bulk triple point T_T was considered. For a temperature T slightly below T_T on the sublimation line, the quantities $\gamma_{SL}(\hat{n})$ and γ_{LV} are not any longer well-defined. However, they can be fixed by extrapolating from higher temperature. For $T < T_T$, the bulk liquid is thermodynamically unstable, i.e. it costs energy to create a liquid lens on the crystal. This can be incorporated if one adds

$$F_t = tA_L \tag{6}$$

to the functional Σ. The physical meaning of t becomes clear in the thermodynamic limit of very large crystals (A_S, $A_L \to \infty$). Then, t equals the difference in bulk free energy between solid and liquid. Hence, in this case, $t = C(T_T - T)$, C denoting a latent heat. Strictly speaking, this is not any longer true for a finite-size system. However, in order to keep the model as simple as possible, it is assumed that the differences in free-energy density between solid and liquid are the same for an infinite- and a finite-size system.

t can also be related to other physical quantities, see below.

The model defined by (1), (2) and (6) neglects interactions of interfaces. This interaction is exponentially (like an inverse power law) as a function of the interface distance for short-range (long-range) interparticle interactions. The range of the effective interface interaction is restricted to atomic distances. If the liquid has macroscopic size, the corrections due to interface interactions are negligible. This is indeed the case very near the triple point. In the opposite case where the thickness of the liquid film is comparable to atomic distances, one can define an effective solid–vapor surface tension $\tilde{\gamma}_{SV}$ by taking the minimum of γ_{SV} and $\gamma_{SL} + \gamma_{LV} + \Delta$ where Δ includes the interface interactions. The crystal shape is then determined by a usual Wulff construction with $\tilde{\gamma}_{SV}$. This method is explicitly used for lead crystallites in section 5.

Another assumption which was made implicitly is that the solid exchanges mass with the liquid but not with the vapor or – in other words – that the crystal/liquid system does not change its size via evaporation and condensation of matter from the gas phase. The dominant process by which equilibrium is achieved then is surface diffusion. For lead this is a reasonable assumption [10].

The equilibrium crystal shape is obtained by minimizing the total free energy, consisting of (1) and (6), with respect to $z_1(x)$, $z_2(x)$ and $z_3(x)$ with constraint (2) of fixed total mass. Before doing that, one should recall the *usual* Wulff construction with only *one* given orientation-dependent surface tension (e.g. $\gamma_{SV}(\hat{n})$). A suitable reference is van Beijeren and Nolden [11]; we adopt their notation with one exception: they set $\rho_S \equiv 1$ whereas we keep ρ_S general, since we have also a liquid density ρ_L. Let us briefly describe the procedure.

The constraint of fixed solid mass M is treated by adding $\lambda(M - \int dx\, z(x))$ to the surface free energy where λ is a Lagrange multiplier [12]. Then, the minimization yields a second-order differential equation in $z(x)$ whose solution is the Legendre transform of the surface tension. This solution has two simple properties: First, it is unique up to translations in z and x, which corresponds to the two free constants of the second-order differential equation. The second feature is that the solution has a simple scaling property: for a different total mass M, the shape of the solution does not change, merely its size is altered by simple scaling and $\lambda^{-2} \propto M$.

The same procedure can be applied to a situation near the triple point as sketched in fig. 1. The constraint of fixed total mass M is incorporated by adding

$$F_c = \lambda(M/\rho_S - A_S - A_L\rho_L/\rho_S)/n \tag{7}$$

to the functional $(\Sigma + F_t)/n$, λ being again a Lagrange multiplier which can also be given a physical meaning, see below.

Let us first minimize with respect to $z_1(x)$, $z_2(x)$ and $z_3(x)$ with *fixed* trijunction (x_0, z_0) and then minimize the resulting free energy with

respect to x_0 and z_0. This gives the minimizing solution.

The minimization with respect to $z_1(x)$, $z_2(x)$ and $z_3(x)$ again yields second-order differential equations which are solved by usual Wulff constructions with $\gamma_{SV}(\hat{\boldsymbol{n}})$, $\gamma_{SL}(\hat{\boldsymbol{n}})$ and γ_{LV} respectively. Here, the solution for the liquid/gas interface is a circle. However, the occurrence of F_t and of two different densities results in different Lagrange multipliers λ for the usual Wulff constructions.

This leads to the following illustration of the minimizing solution of $\Sigma + F_t$ where the symmetry of the crystal is taken into account, see fig. 1. The solution consists of parts of three usual Wulff constructions with $\gamma_{SV}(\hat{\boldsymbol{n}})$, $\gamma_{SL}(\hat{\boldsymbol{n}})$ and γ_{LV}. Let us now describe this illustration of the minimizing procedure:

Choose an arbitrary trijunction point (x_0, z_0). Then draw the usual Wulff line for $z_1(x)$ using $\gamma_{SV}(\hat{\boldsymbol{n}})$ such that it is inversion symmetric with respect to $x \to -x$ and crosses the trijunction, see fig. 1. This procedure fixes the Lagrange multiplier λ which we choose to be nonnegative.

As a second step, draw the usual Wulff line for $z_2(x)$ using $\gamma_{SL}(\hat{\boldsymbol{n}})$ and the Lagrange parameter

$$\lambda(1 - \rho_L/\rho_S) + t \tag{8}$$

as indicated in fig. 1 such that it is inversion symmetric around the symmetry line $\overline{OS}$ and crosses the trijunction point. Two situations are possible: $z_2(x)$ may be "innerconvex" (as indicated in fig. 1) or "innerconcave". The reduced temperature t and the ratio ρ_L/ρ_S determine which situation is actually realized; of course it is that one with minimal surface tension, see also the discussion in section 3. If, by this construction, the trijunction point cannot be crossed, choose other values of x_0 and z_0.

Finally, draw a circle with origin on the line OS and radius

$$R = \gamma_{LV}/|\lambda\rho_L/\rho_S - t| \tag{9}$$

in order to obtain the liquid/gas interface $z_3(x)$. This circle should cross the trijunction and $z_3(x) \geq z_2(x)$ $(x_0 \leq x \leq x_2)$ should be valid, otherwise x_0 and z_0 are to be chosen newly.

Now, the actually realized situation is the minimum over x_0 and z_0 with constraint of fixed total mass M. In this equilibrium situation, there is a balance of forces at the trijunction point [3]:

$$\sum_{i=\mathrm{SV,\,SL,\,LV}} (\gamma_i \hat{\boldsymbol{n}}_i + \partial\gamma_i/\partial\hat{\boldsymbol{n}}_i) = 0. \tag{10}$$

In eq. (10), $\hat{\boldsymbol{n}}_i$ is the normal vector of the i-interface at the trijunction and $\partial\gamma_i/\partial\hat{\boldsymbol{n}}_i$ is a vector perpendicular to $\hat{\boldsymbol{n}}_i$ and of length equal to the rate of change of γ_i with respect to θ. Eq. (10) is the generalization of the well-known Neumann triangle [13,14] for fluid trijunctions with orientation-independent surface tension. This was first pointed out by Herring [3] who also gave the modification of (10) if $\partial\gamma_i/\partial\hat{\boldsymbol{n}}_i$ has to be taken at a cusp of $\gamma_i(\hat{\boldsymbol{n}}_i)$, see ref. [3].

Summarizing, the equilibrium crystal shape consists of three lines of usual Wulff constructions, but with different λ's such that it is the minimum with respect to the trijunction point with constraint of fixed total mass.

The geometry of the situation, illustrated in fig. 1, is fairly general including a solid which is totally covered with its liquid and a nonwet solid. However, a liquid drop is another trivial situation which is not included. Therefore, the surface tension of the solid/liquid system has to be compared with that of a liquid drop in order to obtain the physically realized situation. This can give rise to a first-order phase transition from a situation "solid covered with liquid" to a liquid drop. In our model, finite size effects imply that this phase transition does not occur exactly at $t = 0$ but for a certain $t^* \propto L^{-1}$ where $L \propto \sqrt{M}$ is a typical linear dimension of the solid/liquid system. The same behavior for the shift t^* in the phase transition temperature was found by Lipowsky and Gompper [15] for interface delocalization transitions.

In the variational derivation of the Wulff construction we followed ref. [11]. One could also use the physically more transparent approach from ref. [9]. Then, the Lagrange multiplier acts as an effective chemical potential which is the same in all phases. The curvature of each interface between phases I and J is then related to the difference in pressure, Δp_{IJ}, between the two phases I and J ($I, J = \mathrm{V, L, S}$) by the usual

Laplace law (where in the anisotropic case the surface energy has to replaced by the surface stiffness). The angles at the junction obey eq. (10). Of course, this point of view is completely equivalent to the more mathematical variational strategy. The advantage of the latter is that λ and t can be related [9] to Δp_{IJ}:

$$\lambda = \Delta p_{SV}(\rho_S - \rho_V)/\rho_V,$$

and

$$t = \Delta p_{SL}(\rho_S - \rho_L) /\rho_L - \Delta p_{SV}(\rho_S - \rho_V)(\rho_S - \rho_L)/(\rho_V \rho_S),$$

ρ_V being the vapor density.

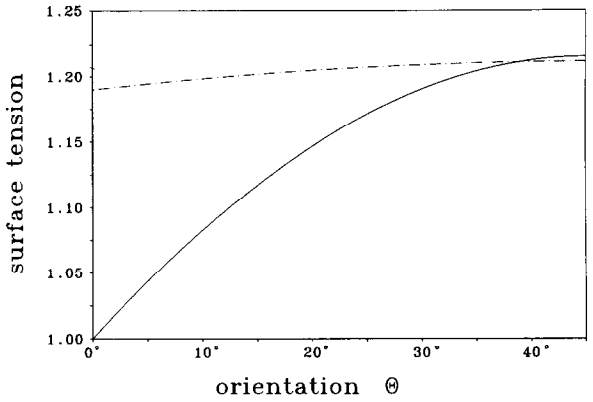

Fig. 2. Surface tensions γ_{SV} (solid line) and $\gamma_{SL} + \gamma_{LV}$ (dashed line) as a function of orientation θ within the simple model. The parameters are $a = 0.52$, $\gamma_0 = 1$, $\gamma_{LV} = 1.09$.

3. Melting of a finite-size crystal

In this section, we present numerical results for the equilibrium shape of a two-dimensional square-lattice crystal near the triple point.

In order to make the model as simple as possible, we assume temperature-independent surface tensions $\gamma_{SV}(\hat{\boldsymbol{n}})$, $\gamma_{SL}(\hat{\boldsymbol{n}})$ and γ_{LV}. In the model, analytical expressions for the surface tensions are used. With $\hat{\boldsymbol{n}} = (\cos\theta, \sin\theta)$ these expressions are

$$\gamma_{SV}(\hat{\boldsymbol{n}}) = \gamma_0\big(1 - a + \sqrt{2}\,a\,\sin(|\theta| + \pi/4)\big), \quad (11)$$

$$\gamma_{SL}(\hat{\boldsymbol{n}}) = w\gamma_{SV}(n), \quad (12)$$

$$\gamma_{LV} = \text{constant}. \quad (13)$$

with $0 \le a \le 1$ and $w = 1/10$, which is the right order of magnitude found in experiments.

Eq. (11) implies that the equilibrium crystal shape consists of lines and a quarter of a circle which match smoothly, see fig. 3a. The number a fixes the ratio of the total facet length and the radius of the circle, this ratio equals $2a/(1-a)$.

In fig. 2, the surface tensions $\gamma_{SV}(\hat{\boldsymbol{n}})$ and $\gamma_{SL}(\hat{\boldsymbol{n}}) + \gamma_{LV}$ are shown as a function of θ. For the chosen parameters $\gamma_{LV}/\gamma_0 = 1.09$, $a = 0.52$, γ_{SV} is smaller (larger) than $\gamma_{SL} + \gamma_{LV}$ for $\theta = 0$ ($\theta = \pi/4$). This means that the closest packed (10) plane does not melt but the looser packed (11) plane does.

In fig. 3 the results of the numerical minimization of the model (11)–(13) are shown for different temperatures.

The typical scenario for finite-size melting is dominated by a competition between free energy and geometry.

First, the situation without liquid is illustrated (fig. 3a). This is a usual Wulff plot with $\gamma_{SV}(\hat{\boldsymbol{n}})$ consisting of facets (lines) and rounded parts (quarters of a circle). Near the triple point, the orientations near the (11) plane do melt and a quasi-liquid film is formed on the crystal surface. Simultaneously, a change in the macroscopic crystal form takes place. This form can be obtained approximately by a Wulff plot with $\min(\gamma_{SV}(\hat{\boldsymbol{n}}), \gamma_{SL}(\hat{\boldsymbol{n}}) + \gamma_{LV})$. The crystal reduces its total length in order to save surface free energy at the expense of higher surface tension at the rounded parts, see fig. 3b.

Starting from this situation, the crystal melts further for increasing temperature in a simple way: The liquid lens becomes larger and grows inwards the crystal. For

$$t_1 = \lambda(1 - \rho_L/\rho_S) \quad (14)$$

the lens changes from "innerconvex" to "innerconcave", see figs. 3c and 3d. Physically, this means that the pressure difference Δp_{SL} vanishes for $t = t_1$.

At a certain t^*, the phase transition to a liquid drop occurs. For $t < t^*$, the situation with a liquid lens corresponds to an overheated crystal. For the chosen parameters in fig. 3, the situations in figs. 3c and 3d are overheated configurations.

The solid/vapor interface of figs. 3b, 3c and 3d is not a plane facet but also contains a small

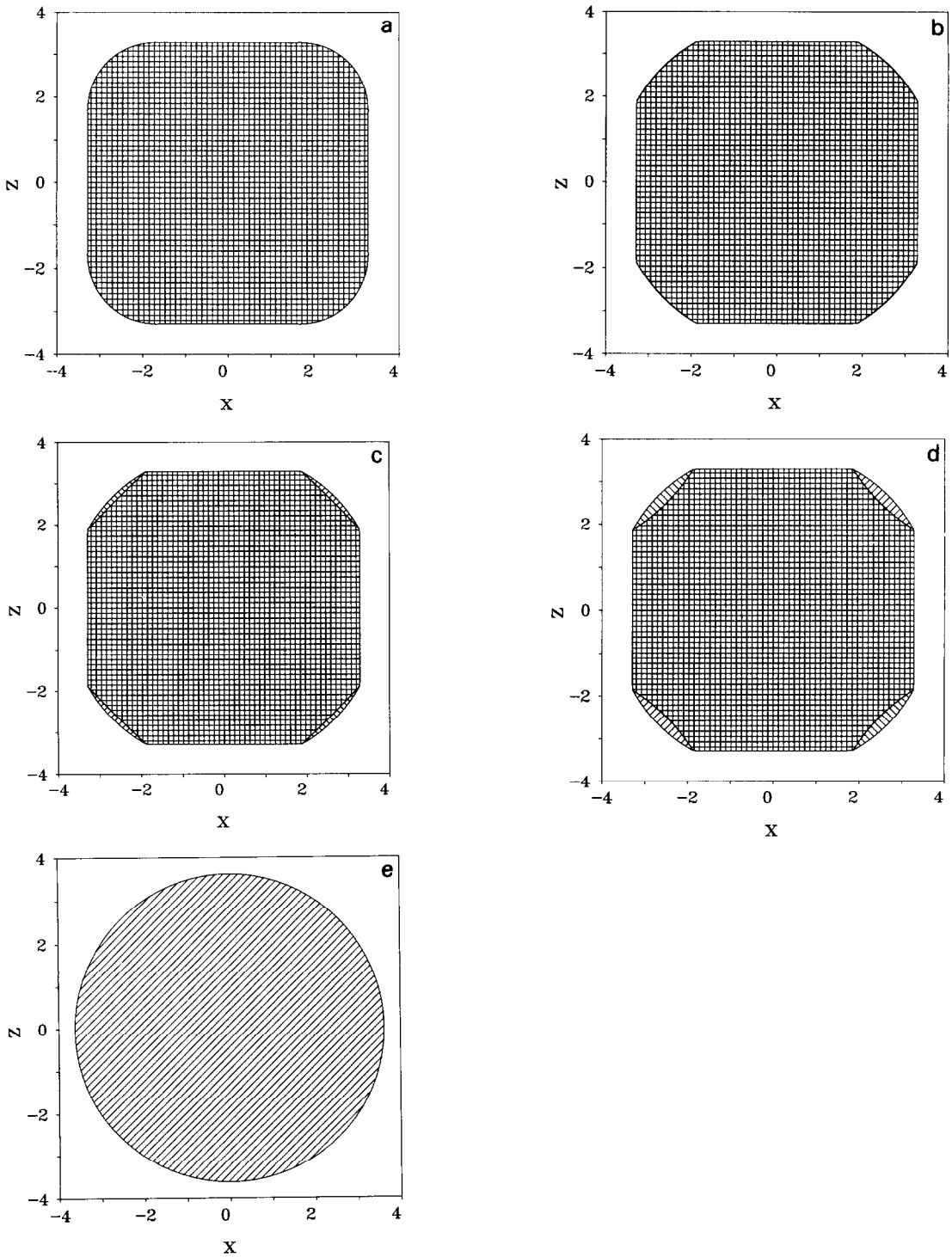

Fig. 3. Equilibrium shapes of a two-dimensional crystal for different temperatures near the triple point in arbitrary units. The parameters of the model are as in fig. 3 and $\rho_S = 1$, $\rho_L = 0.97$, $M = 40$. The double-hatched area corresponds to the solid, the hatched area to the liquid phase: (a) Usual Wulff plot with $\gamma_{SV}(\hat{n})$. (b) Situation with a very thin liquid lens ($t = 0.003$). (c) Emerging of the liquid lens: "innerconvex" situation, $t = -0.007$ (overheated). (d) Emerging of the liquid lens: "innerconcave" situation, $t = -0.02$ (overheated). The transition to a "innerconcave" situation occurs for $t = t_1 = -0.009$. (e) Liquid drop, stable for $t < t^* = 0.0004$.

rounded part near the trijunction which can hardly be seen in the figures. At the trijunction, the liquid lens matches with a finite matching angle to the crystalline part.

An important remark concerns the outer crystal shape involving solid/gas and liquid/gas interfaces. It is this shape which can be seen experimentally. In the simple model where temperature-independent surface tensions were used, this outer shape remains practically constant. As mentioned before, it is given by a usual Wulff construction with $\min(\gamma_{SV}(\hat{n}), \gamma_{SL}(\hat{n}) + \gamma_{LV})$. Therefore a change in this shape with increasing temperature is primarily connected with the temperature-dependence of the surface tensions. This will be useful in section 5.

4. Three-dimensional case

In three spatial dimensions, the trijunction is not a point but a closed line. The simple model, discussed in section 2, can be generalized to three dimensions in a straightforward manner. In general, a simple graphical illustration is lacking in three dimensions. Nevertheless, even in the 3D case, liquid lenses should occur which match with a finite matching angle to the crystalline part.

In order to make the model more realistic, a contribution from the line tension [14] of the trijunction line should be added to the total free-energy functional. The occurrence of the line tension combined with the fact that geometry in three dimensions is more complicated can induce new interesting properties of the crystal equilibrium shape.

It is conceivable that a discontinuous behavior of the equilibrium shape occurs as the temperature is increased. This is connected with a first-order phase transition (i.e. a cusp in the free energy). Such a transition occurs between two different situations: In the first situation, the solid/vapor interface is a connected area with "islands" of liquid/gas interface. In the second situation, this is reversed; now the liquid/vapor interface is a connected area with solid–vapor islands. It is conceivable that such a transition is detectable for lead crystallites $\simeq 25\,^{\circ}\mathrm{C}$ below T_T.

5. Application to lead crystallites

As already discussed in sections 2 and 3, the outer crystal shape which is accessible experimentally can be obtained by a usual Wulff construction with $\min(\gamma_{SV}(\hat{n}), \gamma_2(\hat{n}))$ where $\gamma_2(\hat{n})$ is an effective tension incorporating the solid/liquid and the liquid/vapor interface and the repulsion between them. This was already noted in refs.

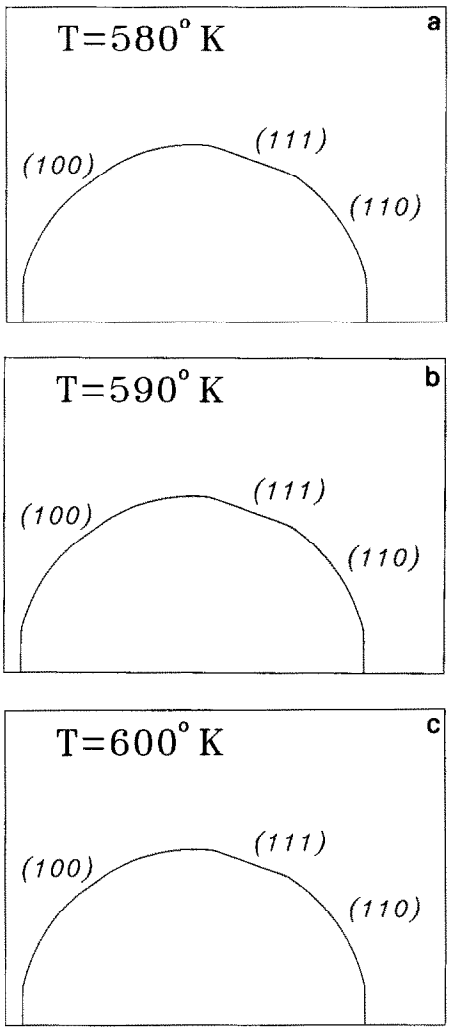

Fig. 4. Equilibrium shape of lead crystallites near the melting point ($T_T = 600.7$ K) for three different temperatures: (a) $T = 580$ K, (b) $T = 590$ K, (c) $T = 600$ K. Only the (110) zone is shown. The increase in the orientation cusp $\Delta\theta$ (which separates a solid and a liquid surface) for increasing temperature is clearly visible. The facet size is not directly visible since it is smoothly connected with a rounded crystalline part.

[5,9]. In this section, we adopt experimental data for $\gamma_{SV}(\hat{\boldsymbol{n}})$ and $\gamma_2(\hat{\boldsymbol{n}})$ in the case of lead and then calculate the outer crystal equilibrium shape. Thus the temperature dependence of the crystal shape is governed by the temperature dependence of $\gamma_1(\hat{\boldsymbol{n}}, T) \equiv \gamma_{SV}(\hat{\boldsymbol{n}})$ and $\gamma_2(\hat{\boldsymbol{n}}, T) \equiv \gamma_2(\hat{\boldsymbol{n}})$. Only for the (110) zone of the fcc lead crystal experimental data are available, so we restrict ourselves to this situation. First, the temperature dependence for the anisotropy $\gamma_1(\hat{\boldsymbol{n}}, T)/\gamma_{111}(T)$ is extrapolated from the data of Heyraud and Métois [10]. Here, T was raised up to $\simeq 27$ K below T_T. Interestingly enough, the derivative of γ with respect to orientation at the (111) facet seems to increase with increasing temperature for $T \gtrsim 550$ K. This quantity determines the (111) facet size; therefore an increase of facet size with increasing T is expected.

Furthermore, from ref. [16], we take

$$\gamma_{111}(T) = \gamma_0^0 - \gamma_1' T, \tag{15}$$

with $\gamma_1^0 = 0.61$ J/m^2, $\gamma_1' = 0.11$ mJ/m$^2 \cdot$ K.

Concerning $\gamma_2(\hat{\boldsymbol{n}}, T)$, we use the empirical rule [17] $\gamma_{SL}(\hat{\boldsymbol{n}}, T) = \gamma_{SV}(\hat{\boldsymbol{n}}, T)/10$ and $\gamma_{LV}(T) = \gamma_2^0 - \gamma_2'(T - T_T)$ with $\gamma_2^0 = 0.501$ J/m^2 (see ref. [8]) and $\gamma_2' = 0.11$ mJ/m$^2 \cdot$ K (see ref. [18]). $\gamma_2(\hat{\boldsymbol{n}}, T)$ is the sum of $\gamma_{SL}(\hat{\boldsymbol{n}}, T)$ and $\gamma_{LV}(T)$ plus corrections due to interface repulsion. We use the form of ref. [8]:

$$\begin{aligned}\gamma_2(\hat{\boldsymbol{n}}, T) &= \gamma_1(\hat{\boldsymbol{n}}, T)/10 + \gamma_{LV}(T) + LN_{eq}(\hat{\boldsymbol{n}}, T)t \\ &\quad + \Delta\gamma(\hat{\boldsymbol{n}}, T)\exp\left[-N_{eq}(\hat{\boldsymbol{n}}, T)/N_0\right],\end{aligned} \tag{16}$$

with

$$\Delta\gamma(\hat{\boldsymbol{n}}, T) = 9\gamma_1(\hat{\boldsymbol{n}}, T)/10 - \gamma_{LV}(T) \tag{17}$$

and

$$\begin{aligned}N_{eq}(\hat{\boldsymbol{n}}, T) &= \mathrm{Max}\{0, N_0 \ln\left[\Delta\gamma(\hat{\boldsymbol{n}}, T)/(tLN_0)\right]\},\end{aligned} \tag{18}$$

where $L = 7.93 \times 10^{-21}$ J, $N_0 = 7.32 \times 10^{18}$ m^{-2}. In eqs. (16) and (18), t is the reduced temperature

$$t \equiv (T_T - T)/T_T \tag{19}$$

and $T_T = 600.7$ K.

By this way, we get a surface tension without any fit parameter. Symmetry arguments ensure us that the crystal shape in the (110) zone is obtained by performing a *one-dimensional* Wulff construction with $\min(\gamma_1(\hat{\boldsymbol{n}}, T), \gamma_2(\hat{\boldsymbol{n}}, T))$, $\hat{\boldsymbol{n}}$ being now the orientation in the (110) zone.

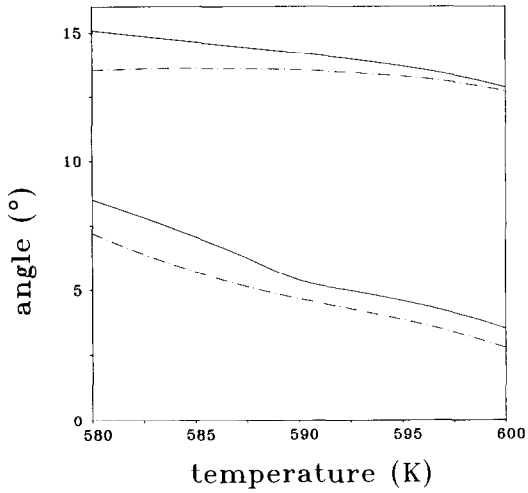

Fig. 5. Lower angle θ_{min} and upper angle θ_{max} at the discontinuity in orientation ($\Delta\theta = \theta_{max} - \theta_{min}$) versus temperature. The full lines are for the direction (111) → (110), the dotted lines are for (111) → (100).

The result is shown in fig. 4 for three different temperatures. Both the (111) facet size d_{111} and the inverse of the central distance h_{111} of the (111) facet increase with increasing temperature. We get explicitly

$$d_{111}/h_{111} = 0.35 - 0.70t, \tag{20}$$

t being the reduced temperature. Starting from the (111) facet, both in (111) → (100) and (111) → (110) direction the orientation is a continuous function up to an angle θ_{min}. Then it jumps discontinuously to an angle θ_{max} with $\Delta\theta = \theta_{max} - \theta_{min}$. This is illustrated in fig. 5. $\Delta\theta$ increases with increasing temperature. Therefore we do not obtain a ring but merely one discontinuity in orientation.

In our approach, the (100) facet does not melt. In contrast to the (111) facet, its size decreases with increasing T.

The increase of d_{111}, $1/h_{111}$ and $\Delta\theta$ with T is in qualitative agreement with the experimental findings [5,7]. The quantitative agreement, however, is less satisfying; for instance d_{111}/h_{111} is larger in experiment compared to (20). At the

melting point, we have $\theta_{max} \simeq 12.8°$. This disagrees with the experimental value of 17° of ref. [5] but agrees with the half-angle 13.5° of the (111) ring as observed in ref. [7]. This is not yet fully understood, see also the discussion in ref. [7].

Of course, our result depends sensitively on the experimental input data. In fact, the experimental error in the data for $\gamma_1(n, T)/\gamma_{111}(T)$, for instance, is rather high [19]. Better measurements are necessary in order to have a more reliable input for the surface tensions near the triple temperature.

6. Conclusions

In conclusion, the Wulff construction was applied to the triple point and properties of the solution were discussed for 2D and 3D crystals. As a result, the equilibrium shape of a crystal can exhibit liquid lenses which reflect the fact that some planes undergo surface melting and others do not. For such a liquid lens, finite angular matching was found which is in qualitative accordance with the experiments.

Furthermore, experimental data for the surface tensions of lead for lower temperatures than T_T were extrapolated to higher T and used as input in order to predict the temperature dependence of the crystal equilibrium shape. It turns out that the (111) facet size and the matching angle between solid and liquid surfaces increase with increasing temperature, which is in qualitative agreement with experiments. However, the quantitative agreement is not satisfying. More experimental and further theoretical studies are necessary to reveal the influence of surface melting on the equilibrium shape of crystals.

In simple effective interface models for planar surface melting, one might get the wrong impression that complete melting means that the whole solid is converted into the liquid phase continuously. However, in these models, one deals with an infinite crystal. In practice, the finite size of a crystal and external wall potentials or gravitational fields [20] lead to a situation at the triple point where (according to Gibb's phase rule) all three phases solid, liquid and gas are present. A continuous melting from the solid surface of a finite-size crystal only takes place if the solid melts for any surface orientation.

Acknowledgments

I thank H. Wagner for a critical reading of the manuscript and for useful discussions. Furthermore, I have benefited from discussions with B. Widom, P. Nozières, R. Lipowsky, H.P. Bonzel, E. Bauer, J.J. Métois and T. Beier.

References

[1] G. Wulff, Z. Krist. 34 (1901) 449.
[2] A. Dinghas, Z. Krist. 105 (1944) 304.
[3] C. Herring, in: Structure and Properties and Solid Surfaces, Eds. R. Gomer and C.S. Smith (University of Chicago Press, Chicago, 1953).
[4] J.J. Métois and J.C. Heyraud, Ultramicroscopy 31 (1989) 73.
[5] J.C. Heyraud, J.J. Métois and J.M. Bermond, J. Cryst. Growth 98 (1989) 355.
[6] J.J. Métois and J.C. Heyraud, J. Phys. (Paris) 50 (1989) 3175.
[7] A. Pavlovska, K. Faulian and E. Bauer, Surf. Sci. 221 (1989) 233.
[8] B. Pluis, A.W. Denier van der Gon, J.W.M. Frenken and J.F. van der Veen, Phys. Rev. Lett. 59 (1987) 2678.
[9] P. Nozières, J. Phys. (Paris) 50 (1989) 2541.
[10] J.C. Heyraud and J.J. Métois, Surf. Sci. 128 (1983) 334.
[11] H. van Beijeren and I. Nolden, in: Structure and Dynamics of Surfaces II, Eds. W. Schommers and P. von Blanckenhagen, Vol. 43 of Topics in Current Physics (Springer, Berlin, 1987).
[12] Note that in ref. [11] a factor 2 is present since there three-dimensional situations are studied whereas I focus on two-dimensional crystals.
[13] F. Neumann, Vorlesungen über die Theorie der Capillarität, Ed. A. Wangerin (Teubner, Leipzig, 1894) ch. 6, §1.
[14] J.S. Rowlinson and B. Widom, Molecular Theory of Capillarity (Clarendon, Oxford, 1982).
[15] R. Lipowsky and G. Gompper, Phys. Rev. B 29 (1984) 5213.
[16] A.R. Miedema, Z. Metallkd. 69 (1978) 287.
[17] See, for example, A.R. Miedema and F.J.A. den Broeder, Z. Metallkd. 70 (1979) 14.
[18] A.R. Miedema and R. Boom, Z. Metallkd. 69 (1978) 183.
[19] J.J. Métois, private communication: Although clearly visible in fig. 5 of ref. [10], the increase of the derivative of $\gamma_1(n, T)/\gamma_{111}(T)$ with respect to orientation at the (111) facet with increasing temperature is not completely significant in the measurement.
[20] H. Löwen and T. Beier, Z. Phys. B 79 (1990) 441.